scientific reports



OPEN

Intratracheal instillation of RSV is superior to intranasal inoculation as a model method inducing critical immune cell infiltration

Yinglin Lin^{1,3}, Yao Xiao^{1,3}, Bin Peng^{1,3}, Mengyuan Xie^{1,3}, Zesen Mai¹, Mingzhen Lin¹, Shanshan Miao¹, Xinru Yang¹, Wei Li¹, Yi Wang², Zhaoyu Liu^{1⊠} & Wenxia Yao^{1⊠}

Respiratory syncytial virus (RSV) causes a substantial global disease burden, particularly in children and older adults. Despite the availability of three vaccines and two prophylactic monoclonal antibodies, there remains an urgent unmet need for effective RSV treatments. Appropriate experimental animal models and modeling methods are essential for studying RSV pathogenesis and developing therapeutic and preventive agents. In this study, we introduced intratracheal instillation (ITS) method into mouse model of RSV infection and compared it with the conventional intranasal inoculation (INO) method; data showed that ITS method resulted in more efficient viral replication and more severe pathological changes than INO method. Then RNA-seq technology was used to sequence the lung tissues of RSV infected mice with ITS method, and further immunoinfiltration analysis based on transcriptomic profile demonstrated that the ITS approach can lead to the infiltration of multiple innate and adaptive immune cells. It is concluded that ITS of RSV is superior to INO as a model method in mice and can induce infiltration of key immune cells. Collectively, our study offers novel insights into the rational design of future in vivo infection methods with RSV, as well as providing a foundation for the investigation of the immune pathogenesis of RSV.

Keywords RSV, Modeling method, Intratracheal instillation, Immune infiltration

Respiratory syncytial virus (RSV) causes widespread respiratory infections worldwide and is recognized as one of the most prevalent and serious respiratory pathogens in children¹. Vulnerable populations primarily include infants, the elderly and immunocompromised individuals. Globally, approximately 33.1 million children are infected with RSV annually². Due to its high mutation rates as an RNA virus, RSV presents challenges in disease control and leads to recurrent infections³. Currently, there are no approved small molecule drugs to treat RSV infections, which contribute to approximately 150,000 annual deaths globally, with the majority occurring in developing countries². Although three vaccines and two prophylactic monoclonal antibodies have been approved, RSV treatment represents a clear unmet medical need^{4,5}. In conclusion, RSV imposes a serious global disease burden, underscoring the critical need for further exploration into its pathogenicity and molecular mechanisms.

Understanding the molecular and cellular mechanisms of RSV infection is critical for developing effective and safe therapeutic and preventive agents^{5,6}. Experimental animal models are essential for this development. The selection of appropriate animal models for RSV is crucial for investigating viral pathogenesis and developing treatment strategies⁷. Previous studies have employed various animal models to study RSV infection, including mice, cotton mice, chimpanzees, cattle, and sheep. Due to the ease of care, low cost, and the availability of scientific tools, mice are frequently used to model RSV infection^{3,8}.

RSV is primarily transmitted through contact with virus-containing secretions or pollutants from the nasopharyngeal mucosa or the mucous membranes of the eyes³. Direct contact is the most common route of transmission, but droplets and aerosols can also cause transmission¹⁰. Different infection routes/methods for

¹Key Laboratory of Biological Targeting Diagnosis, Therapy and Rehabilitation of Guangdong Higher Education Institutes, GuangDong Engineering Technology Research Center of Biological Targeting Diagnosis, Therapy and Rehabilitation, State key Laboratory of Respiratory Disease, The Fifth Affiliated Hospital, Guangzhou Medical University, The Fifth Clinical College of Guangzhou Medical University, Guangzhou, China. ²Dongguan Key Laboratory for Zoonitic Diseases, Dongguan Bioshine Technology Company, Dongguan City, China. ³Yinglin Lin, Yao Xiao, Bin Peng and Mengyuan Xie contributed equally to this work. [™]email: gywyer@gzhmu.edu.cn; yaowenxia917@gzhmu.edu.cn

pathogens other than RSV usually yield different research outcomes. For example, lung injury and viral load in mice differ following intratracheal versus intranasal administration of influenza virus¹¹. Similarly, disease manifestation and mortality patterns in ferrets vary following intranasal versus intratracheal infection^{7,12}. In murine models of RSV infection, the predominant method of infection was intranasal inoculation. Previous research¹³ assessed multiple pathological and immunological parameters in BALB/c mice following intratracheal intubation (ITT) and intranasal inoculation (INO) of RSV-A2; the research found that INO elicited more severe pathology and inflammation than ITT, suggesting its superiority in RSV infection studies. Besides ITT, intratracheal instillation (ITS) technology is also used to deliver a variety of agents to the lungs, ranging from pathogens and toxins to therapeutic agents¹⁴. Natural human coughing is better mimicked by ITS, which results in the lungs being filled with the virus in large amounts within a short time. Direct lung infection by respiratory viruses under simulated aspiration conditions should not be underestimated. Our preliminary findings corroborate the aforementioned conclusions ITS results in broader pulmonary viral dissemination compared to ITT during viral challenge. Furthermore, ITT causes substantial airway trauma, thereby precluding its suitability as a modeling approach. ITS has been successfully utilized in modeling adenovirus infection in the lungs¹⁵. However, its application in the modeling of RSV infection has not been reported, nor has it been compared with INO in the case of RSV infection.

RNA sequencing (RNA-seq) is a high-throughput technology that enables comprehensive and quantitative analysis of gene expression profiles in specific tissues or cells under defined experimental conditions. It serves as a powerful tool for gaining profound insights into biological processes, disease mechanisms and drug development¹⁶. Immunoinfiltration analysis assesses immune cell infiltration in tumors or tissues to reveal the pivotal role of immune cells in disease occurrence, development, and treatment response¹⁷. Immunoinfiltration analysis elucidates the distribution, quantity and function of different immune cell subsets in specific tissues, thereby providing novel insights into disease diagnosis and treatment. RNA-seq provides a rich data source for immune infiltration analysis due to its capability to yield extensive gene expression profiles. RNA-seq provides a robust data foundation for immunoinfiltration analysis owing to its capability to generate comprehensive gene expression profiles. Through RNA-seq data, the type, quantity and functional status of immune cells in tissues can be inferred indirectly, thus achieving a comprehensive assessment of immune infiltration¹⁸. Based on this rationale, we utilized RNA-seq to characterize pulmonary immunoinfiltration patterns in RSV-infected murine models.

In this study, we introduced the ITS method into murine model of RSV infection and performed comparative analysis with the conventional INO method; data showed that ITS method resulted in more efficient viral replication and more severe pathological changes than INO method. Subsequent RNA-seq technology was used to sequence the lung tissues of mice infected by RSV with ITS method, and further immunoinfiltration analysis based on transcriptomic profile demonstrated that RSV infection in mice with the ITS approach can model and replicate major immune infiltration observed in humans, including the infiltration of multiple innate and adaptive immune cells.

Materials and methods Cells and virus

HEp-2 cells (ATCC CCL-23) were cultured in Dulbecco's minimal essential medium (DMEM) supplemented with 10% fetal bovine serum (FBS; HyClone) and 1% penicillin-streptomycin¹⁹. The cells were maintained at 37 °C in a humidified atmosphere containing 5% CO2. RSV (A2 strain) was propagated in HEp-2 cells for large-scale preparation. UV-inactivated RSV was generated by exposing the RSV virus to UV radiation for 2 h.

RSV Titration

To determine the viral titer, HEp-2 cell monolayers were incubated with serial dilutions of the virus supernatants for 120 min at 37 °C and then overlaid with medium containing 2% FBS and 1% methylcellulose. At 3 days postinfection (dpi), the cells were fixed with 4% polyformaldehyde for 15 min. Subsequently, fluorescent plaques formed through specific antibody binding were observed under a microscope. Plaques were visualized and counted.

Mice

Specific-pathogen-free female BALB/c mice, aged 6-8 weeks, were obtained from Guangdong Medical Experimental Animal Center (SCXK(yue)2022-0002) and maintained under standard approved conditions. The mice were fed for one week after arriving in the laboratory to ensure that the mice were normal in weight and health when immunized. Finally, we euthanized mice using an overdose anesthesia method of intraperitoneal injection anesthesia with 3% sodium pentobarbital 60 mg/kg body weight. In our animal experiments, we strictly adhere to the 3Rs principles (Replacement, Reduction, and Refinement). Based on these principles, we calculated the required sample size to ensure statistical validity while minimizing animal use. To further uphold ethical standards, all procedures incorporate comprehensive pain management strategies, including appropriate analgesia and anesthesia. Additionally, predefined humane endpoints are established to promptly euthanize animals showing severe distress or irreversible suffering, ensuring their welfare is prioritized throughout the study. The calculations showed that a sample size of approximately n = 5 is needed for 90% detection power, n = 4for 80%, and n = 3 for 70%. Consequently, we chose a group size of 5 mice per experimental group. However, due to uncontrollable factors, such as unexpected mouse deaths or the occurrence of outliers, the actual number of mice in the presented data ranged from 3 to 5, ensuring a detection power exceeding 70%. All participants in the experiment had the qualifications and skills to carry out the corresponding animal experiments. The study was approved by the Institutional Animal Care and Use Committee on animal welfare (IACUC No. HTSW221144). This study was conducted in accordance with the ARRIVE guidelines.

Infection of mice

The animals were randomly divided into groups. The blank group consisted of mice that did not undergo any treatment. Mice in the RSV groups were infected with $100~\mu L$ of 1×10^7 PFU RSV, while mice in the mock groups were infected with $100~\mu L$ of 1×10^7 PFU UV-inactivated RSV. The mice were sacrificed and sampled at 0, 1, 4, 7, and 10 days post infection, and the samples were taken, including lung tissue, trachea tissue and turbinate bone tissue. Bodyweight was measured every day until mice were euthanized.

Determination of viral titer in mouse lung tissue by Immunofluorescence

After euthanizing the mice, fresh lung tissue was collected and mixed with pre-cooled 2% DMEM. The mixture was placed in pre-cooled EP tubes containing two magnetic beads. The tissue was homogenized in a pre-cooled tissue homogenizer at a frequency of 50 Hz for 30 s, repeated twice. The homogenate was then centrifuged at 4000 g for 15 min at 4 °C in a micro high-speed refrigerated centrifuge (Beckman Coulter, USA). The supernatant was collected and used to determine the viral titer of RSV in mouse lung tissue using the aforementioned immunofluorescence titration method.

RNA preparation, reverse transcription and real-time PCR

After euthanizing the mice, fresh lung tissue, turbinate bone tissue, and tracheal tissue were collected separately and stored in RNA preservation solution (Thermo Fisher, Thermo Fisher Scientific, Shanghai Trade Co.) at -80 °C for further research. Total RNA was extracted from the tissues using TRIzol reagent (Yishan Biotech, Shanghai Yishan Biotech Co., Ltd.). The RNA was then reverse transcribed into cDNA using HiScript IV All-in-One Ultra RT SuperMix for qPCR (Vazyme, Nanjing Vazyme Biotech Co., Ltd.). RSV (Forward: TCTGTCATC CAGCAAATACACC; Reversed: TGTTTCTGCACATCATAATTAGGA), IL-6 (Forward: TGGAGTCACAGAA GGAGTGGCTAAG; Reversed: TCTGACCACAGTGAGGAATGTCCAC), IL-10 (Forward: TGGCTCCTAGC ACCATGAAG; Reversed: CGCAGCTCAGTAACAGTCCG), and MIG (Forward: TGCTAGAGGCAAAAACT CTGTG; Reversed: TAGGCTCAAGGGCGTGAT) expression was detected using ChamQ SYBR qPCR Master Mix (Low ROX Premixed) (Vazyme, Nanjing Vazyme Biotech Co., Ltd.) in a PCR instrument (Biosystem 7500). β-actin (Forward: TGGCTCCTAGCACCATGAAG; Reversed: CGCAGCTCAGTAACAGTCCG) was used as the internal reference.

Histopathology

In order to evaluate lung pathology, the right lower lobe of the mouse lung was taken and immersed in 4% paraformaldehyde for one day. Fixed lungs were embedded in paraffin blocks, sectioned, and stained with hematoxylin and eosin (H&E).

Library Preparation and sequencing

Total RNA of lung samples was extracted using TRIzol (Invitrogen) according to the manufacturer's instructions. RNA quantity and purity were analyzed with an RNA integrity number (RIN) of >7.0. After extraction, total RNAs were subjected to rRNA removal prior to library preparation. Library construction and RNA sequencing were performed at the Gene Denovo Biotechnology Company (Guangzhou, China).

Evaluation of infiltrating immune cells

CIBERSORT is a gene expression-based deconvolution algorithm, and it uses a set of gene expression values for characterizing immune cell composition²⁰. Based on the RNA-seq data, CIBERSORT and CIBERSORT-ABS were used to analyze lung tissue immune infiltrating cells, namely: B cell naive, B cell memory, B cell plasma, T cell CD4⁺ naive, T cell CD4⁺ memory resting, T cell CD4⁺ memory activated, T cell follicular helper, T cell regulatory (Tregs), T cell gamma delta, NK cell resting, NK cell activated, Monocyte, Macrophage M0, Macrophage M1, Macrophage M2, Myeloid dendritic cell resting, Myeloid dendritic cell activated, Mast cell activated, Mast cell activated, Mast cell resting, Eosinophil, and Neutrophil.

Statistical methods

The data in the figures represent mean \pm standard deviation (SD). All data were analyzed using GraphPad Prism software. Comparisons between two groups were performed using an unpaired Student's t-test. Multiple comparisons were analyzed using a one-way analysis of variance (ANOVA). *P* values were calculated, and statistical significance was expressed as highly significant with *P<0.05, **P<0.01, ***P<0.001.

Results

Establishment of RSV "infection" model in mice

To validate the operational accuracy during modeling and ensure smooth delivery of the virus solution into mouse lung tissue, we employed a 0.5% Evans blue solution as a surrogate for the virus²¹. "Infection" modeling was achieved through three methods: intranasal inoculation (INO), intratracheal instillation (ITS), and intratracheal intubation (ITT) (Fig. 1A; Table 1). Viral "infection" area was assessed by observing the distribution of the dye solution within the lung tissue. After mice "infection" with 0.5% Evans blue solution for 10 min, mice were dissected to remove the lungs for examination of tissue staining. As shown in figure (Fig. 1B), Evans blue solution can be delivered into lung tissue by all three inoculation methods; however, significant differences were noted in the extent of lung tissue staining among the groups. The staining area of ITT group is the smallest, covering approximately 10% of the total lung tissue area. In contrast, the INO group showed more extensive staining, about 40-50%, while the ITS group had the most, nearly encompassing the entire lung. Additionally, statistical comparison of dye dispersion patterns was provided (Fig. S1). And, higher RNA expression levels and viral titers of RSV were found in the lung tissues of mice infected via ITS compared to ITT in our preliminary

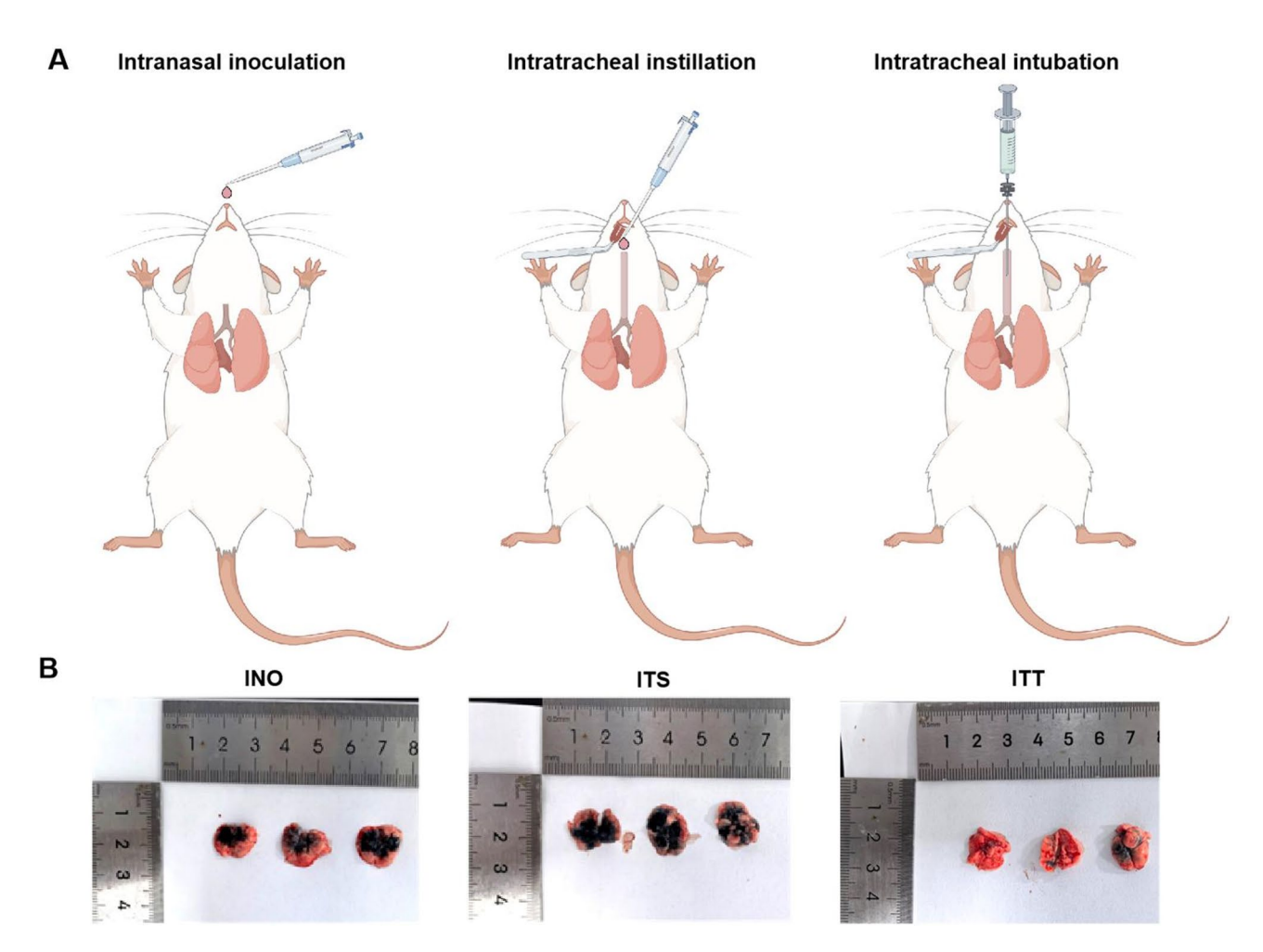


Fig. 1. Schematic figure of the three modeling methods and the dispersal of Evans Blue dye in the lung. (**A**) the simulated models were INO model, ITS model and ITT model by Figdraw (www.figdraw.com), and (**B**) lung tissue samples in vitro (3 mice in each model method) were INO, ITS and ITT group.

Term	Description
INO	Intranasal inoculation (INO): maintain the mouse in a vertical head-torso position parallel to the ground; administer the liquid alternately to each nostril using a micropipette.
ITS	Intratracheal instillation (ITS): secure the mouse in an upright position on an intubation stand; gently extract and fix the tongue with forceps while occluding the nares to open the airway; deliver the liquid directly into the oropharyngeal cavity using a micropipette.
ITT	Intratracheal intubation (ITT): position the vertically restrained mouse on the intubation platform; after visualizing the glottis with a rodent laryngoscope, insert the endotracheal cannula during inspiration; confirm proper tracheal placement before liquid administration through the cannula channel.

Table 1. Glossary explaining the abbreviations of modeling method used, as well as the operating procedure.

experimental research (**Fig. S2**). Furthermore, previous study by Erp et al. with RSV-A2 demonstrated that INO induced more severe pathological changes and inflammatory responses than ITT^{13} . Collectively, all these data suggest that INO and ITS are the more suitable infection methods than ITT. Subsequent studies will use these two methods to further explore the viral infection in mice.

Effective RSV infection in mice by both INO and ITS modeling methods

In this study, female BALB/c mice, aged 6-8 weeks, were randomly assigned to either the INO or ITS treatment. Within each modeling group, mice were further divided into RSV and mock groups. The RSV group received $100 \,\mu\text{L}$ of $1 \times 10^7 \,\text{PFU}$ RSV, whereas the mock group was treated with $100 \,\mu\text{L}$ of $1 \times 10^7 \,\text{PFU}$ UV-inactivated RSV. Modeling success was initially assessed by monitoring changes in body weight and RSV RNA levels in multiple tissues post-infection. Body weights were recorded daily starting from the day of infection (day 0). The weight of mice in the two RSV groups continued to decrease after infection with RSV and began to recover at 4 days post-infection (dpi), while the weight of mice in the mock group continued to decrease for 2 days after infection with RSV and began to recover at 3 dpi (Fig. 2A). Additionally, RT-qPCR was used to detect RSV RNA levels

in lung tissue, turbinate bone and trachea, and robust RSV RNA expression was confirmed in both RSV groups after infection (Fig. 2B-D). These results demonstrate that both modeling methods effectively establish murine models of RSV infection.

ITS induced more severe pathological changes than INO

To investigate the pathological changes in mouse lung tissue at different time following RSV infection via two infection methods, lung tissues from both groups were collected at 1 dpi, 4 dpi, 7 dpi and 10 dpi. Sections were stained with H&E and observed using a fluorescence microscope. Pathological changes including inflammatory cell infiltration around bronchi and blood vessels, lung tissue structure disorder, edema and thickening of alveolar septum resulting in small alveolar cavity were observed at 4 dpi and 7 dpi in both INO and ITS groups (Fig. 3A-B). The severity of pathological injury peaked at 7 dpi in both groups and returned to normal levels at 10dpi. Importantly, we observed significantly more severe lung tissue pathology in the ITS group compared to the INO group at 4 dpi and 7 dpi, characterized by extensive loss of alveolar structures, extensive lymphocyte infiltration around the alveolar walls and blood vessel walls, and disordered lung tissue structure. These results indicate that ITS induced more severe pathological changes in mice than INO.

ITS method resulted in more efficient viral replication compared to the INO method

We then examined the differences induced by the two distinct RSV infection models in vivo. According to the daily body weight trend chart of mice, both the INO and ITS group mice exhibited continued weight loss over the 3 days post-RSV infection (Fig. 4A). Normalizing the initial weight of all mice on day 0, we observed a 20% decrease in weight for the ITS group at 3 dpi, compared to less than 10% in the INO group, indicating significantly greater weight loss in the ITS group at this time point.

To compare the effects of model methods on viral infection, we used RT-qPCR and immunofluorescence assays to monitor viral replication dynamics in the lungs of RSV-infected murine models. First, the viral load of mouse lung was measured by immunofluorescence detection of viral plaques. We found that at 4dpi, viral titers were 1.37×10^5 PFU/g for ITS and 2.81×10^4 PFU/g for INO group (Fig. 4B). It can be seen that the virus titers in lung tissue of mice in the ITS group were higher than that in the INO group (Fig. 4B). Additionally, RT-qPCR was used to evaluate the amount of viral RNA level in lung tissues. The results showed that the expression of viral RNA in mice in the ITS group was significantly higher than that in the INO group at 1, 4 and 7 dpi (Fig. 4C). RSV RNA could be detected in mice in the ITS group at 1 dpi, 4 dpi and 7 dpi, with the largest expression level at 4 dpi (Fig. 4C). In the ITO group, no RSV RNA was detected at 1 dpi or 10 dpi, weak RSV gene expression was detected at 7 dpi, and obvious RSV RNA expression was detected at 4 dpi (Fig. 4C). Simultaneously, viral RNA level in turbinate bone and tracheal tissue was detected. The findings indicated consistently higher RSV RNA expression in these two tissues of the ITS group compared to the INO group across all time points (Fig. 4D and E).

These results collectively demonstrate that the ITS method led to more efficient viral infection and replication compared to the INO method.

Transcriptome sequencing data was validated by RT-qPCR

We then employed RNA-seq to investigate transcriptional changes within the ITS infection group. RSV infection has been reported to lead to the dysregulated expression of multiple inflammatory cytokines in both natural human infection and murine models²². In this study, to verify the reliability of the RNA-seq data, the gene expression levels of interleukin-6 (IL-6), interleukin-10 (IL-10), and chemokine ligand 9 (CXCL9) at 1 dpi, 4 dpi, 7 dpi, and 10 dpi were analyzed in the RNA-seq data (Fig. 5A). Then RT-qPCR was used to detect the expression of IL-6, IL-10 and CXCL9 in lung tissue RNA during the four days (Fig. 5B). The data showed that upon RSV infection, IL-6 and IL-10 had peak expression mainly at 1 dpi, whereas CXCL9 showed peaks at both 1dpi and 7dpi (Fig. 5A-B). It was noted that the expression patterns of RT-qPCR data were consistent with the transcriptome results. Therefore, the accuracy of RNA-seq data was verified.

The proportions of infiltrating immune cells were changed upon RSV infection with ITS method

Subsequently, the cell compositions of immune cell types were estimated from each transcriptomic profile utilizing the CIBERSORT algorithm. Immune cells play a crucial role in fighting viruses, and the immune responses elicited by different cell types vary. RSV infection induces various host antiviral responses, including innate and adaptive immune responses. Initially, following RSV infection, respiratory epithelial cells recognize viral pathogen-associated molecular patterns (PAMPs) through pattern recognition receptors (PRRs). This recognition activates downstream signaling pathways, such as NF-κB and IRF3, leading to the production of early inflammatory mediators²³. The infiltration of different types of innate immune cells is further induced by these inflammatory mediators through various pathways²⁴. The adaptive immune response is also an important part of the immune mechanism in RSV. In this study, by analyzing the immune cells in the lung tissues of mice infected with RSV, we identified the changes in immune cells in the lung tissues of mice after RSV infection. Compared with blank group and mock group, the proportion of macrophage in RSV infection group significantly increased at 1 dpi, peaked at 4 dpi, and gradually decreased at 7 dpi and 10 dpi; and neutrophil infiltration proportion in RSV infection group was significantly higher at 1 dpi and 4 dpi compared to the 7 dpi and 10 dpi (Fig. 6A-C); additionally, the proportion of B cells and T cells decreased at 1 dpi and 4 dpi and then recovered to exceed 50% at 7 dpi and 10 dpi (Fig. 6A-C). These findings indicated that innate immune responses primarily dominate in mouse lung tissues from days 1 to 4 post-infection, while adaptive immune responses become prominent from day 7 onwards.

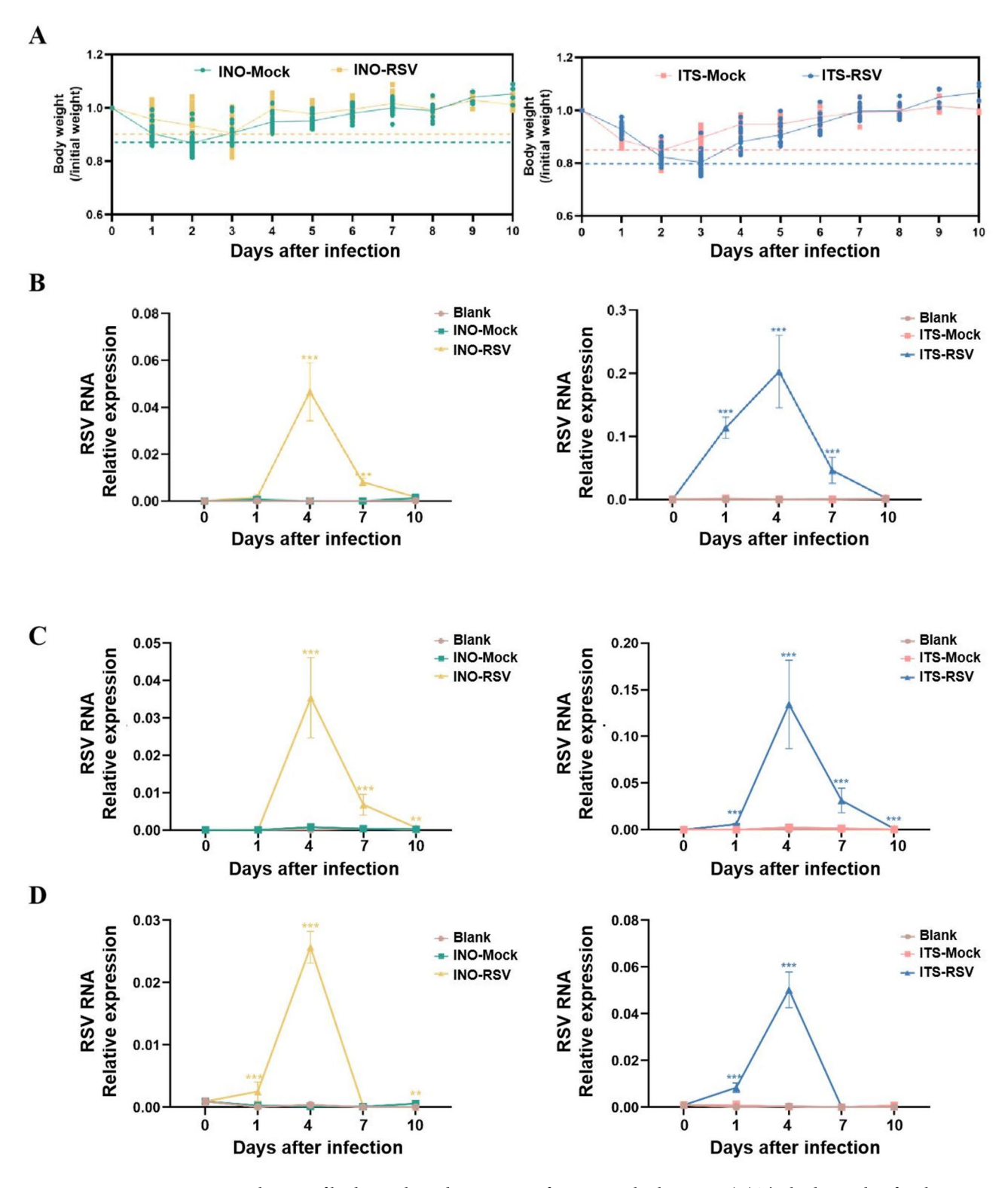


Fig. 2. Changes of body weight and expression of RSV in multiple tissues. (**A**) The body weight of each mouse in each day (weighed at the same time every day). The picture on the left shows the mice in the INO and on the right shows the mice in the ITS. (**B**) RT-qPCR was used to detect the changes of RSV expression in the lung tissue of mice at each time point. (**C**) RT-qPCR was used to detect the changes of RSV expression in the turbinate bone of mice at each time point. (**D**) RT-qPCR was used to detect the changes of RSV expression in the trachea of mice at each time point. (1 mouse in the blank group, $n \ge 3$ mice in the RSV group and mock group).* denotes the degree of significance, *P < 0.05, *P < 0.01, **P < 0.001.

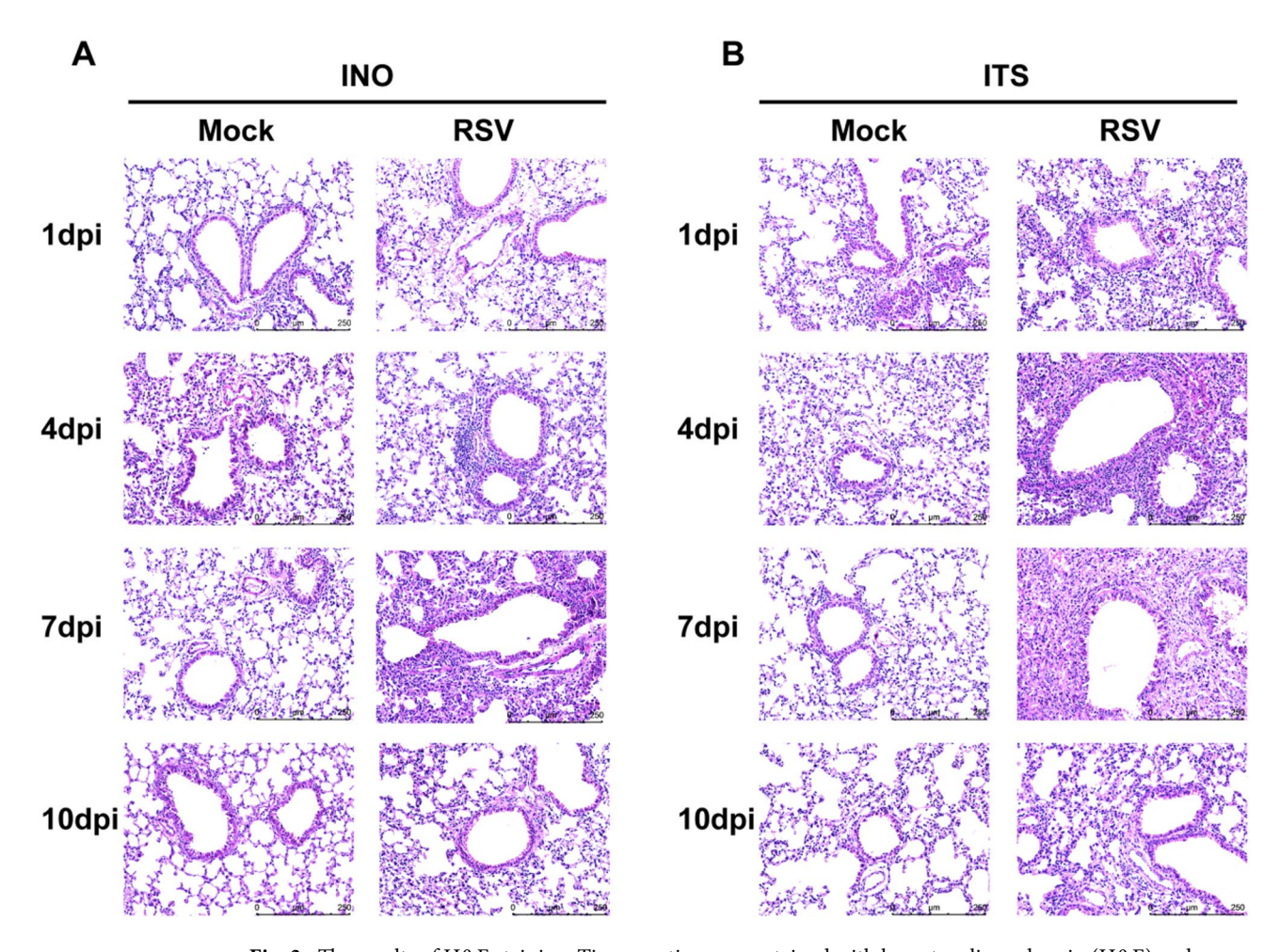


Fig. 3. The results of H&E staining. Tissue sections were stained with hematoxylin and eosin (H&E) and examined under a light microscope ($100 \times \text{magnification}$). One representative H&E-stained section image was selected from three images taken for each group. (A) Results of H&E staining of lung tissue at different time points in INO group. (B) Results of H&E staining of lung tissue at different time points in ITS group.

RSV infection with ITS method led to infiltration of important immune cells

The above results using CIBERSORT provide a comprehensive overview of the proportions of infiltrating immune cells, as shown in the pie charts (Fig. 6), with the total sum equal to 1. We further utilized the CIBERSORT-ABS algorithm to evaluate the infiltration levels of immune cells in both the blank and infected group of mice at different time points. The results are presented in bar charts, highlighting statistical significance. We further utilized the CIBERSORT-ABS algorithm to evaluate the infiltration levels of immune cells in both the blank and infected group of mice at different time points. The results are presented in bar charts, highlighting statistical significance. Results demonstrated that macrophages in the RSV infection group showed significant increases at 1, 4, 7, and 10 dpi, with the most pronounced increase observed at 1 dpi (Fig. 7A); neutrophils in the RSV infection group also significantly increased at 1, 4, and 7 dpi, with the largest increase observed at 1 dpi (Fig. 7B); NK cells in the RSV-infected group showed a significant increase only at 1 dpi compared to the blank group (Fig. 7C); CD8+ T cells in the RSV-infected group exhibited a significant increase at 10 dpi compared to the blank group (Fig. 7D).

Taken together, macrophages, neutrophils, and NK cells, crucial components of innate immunity, exhibited substantial infiltration during the early stage of RSV infection, whereas CD8⁺ T cells, key effector of adaptive immunity²⁵, showed significant infiltration during later stage of infection.Moreover, in the H&E-stained tissue sections from animal experiments, we quantified neutrophil infiltration. The observed variation pattern was consistent with the neutrophil-related changes detected by RNA-seq, further validating the accuracy of the RNA-seq data (Fig. S3).

Discussion

Currently, RSV infection and spread are considered as serious concerns posing potential risks to susceptible populations. Despite ongoing research efforts to understand the pathogenesis and virulence of RSV for developing effective treatments, there are still no specific drugs or broadly applicable vaccines for RSV^{25,26}. Therefore, further research into RSV is imperative. Finding suitable animal models and effective infection methods is crucial for advancing RSV research. Mice are frequently used to model RSV infection, but they

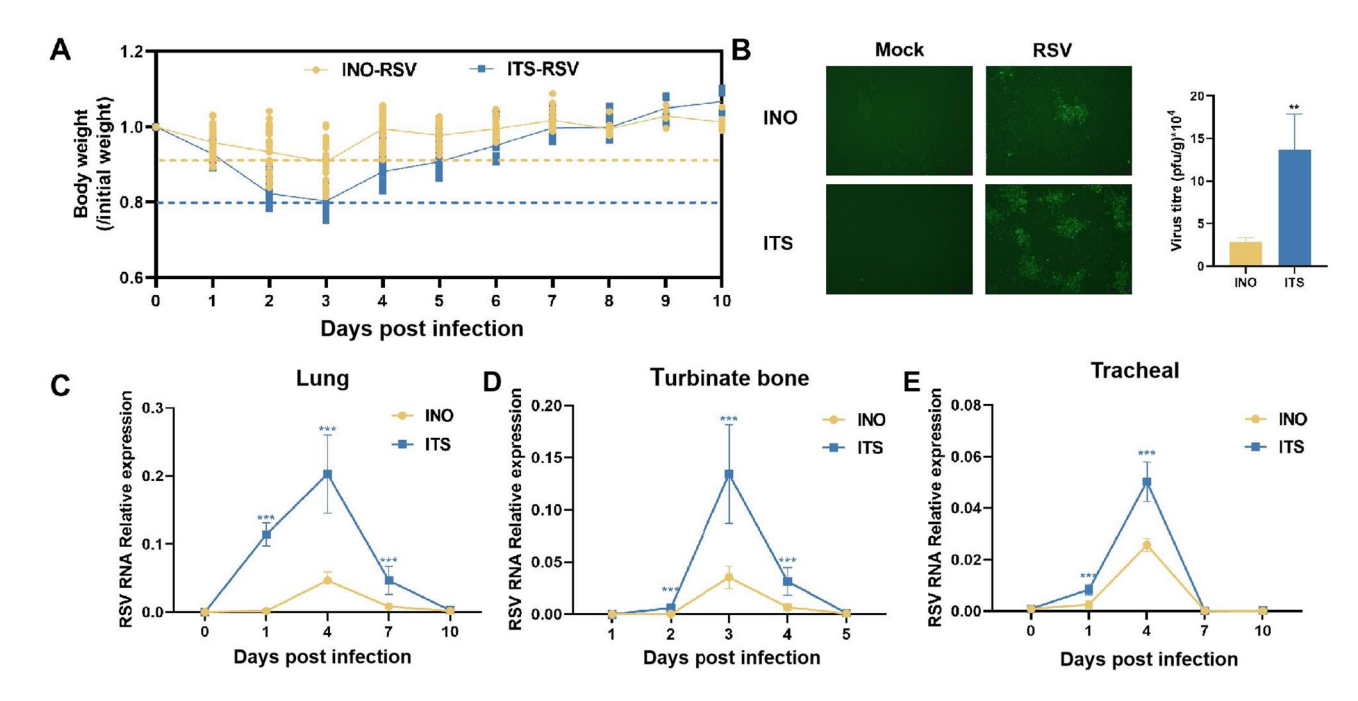


Fig. 4. Comparison of RSV infected mice with two kinds of modeling methods. (**A**) The daily body weight changes of mice in the two RSV infection groups, the solid line is the dotted line of the average daily body weight of mice. (**B**) The virus titer was detected by immunofluorescence in mouse lung tissue. Plaques were counted in three randomly selected fields under a fluorescence microscope at 200× magnification, and the viral titer (PFU/g) was calculated as: (mean plaques/well × dilution factor⁻¹)/inoculum mass (g). The left picture shows the microscopic fluorescence result, and the right picture shows the calculated virus titer result. (**C**) RT-qPCR was used to detect the changes of RSV expression in lung tissue of RSV infected mice ($n \ge 4$ mice in each group at each time point). (**D**) RT-qPCR was used to detect the changes of RSV expression in turbinate bone tissue of RSV infected mice ($n \ge 4$ mice in each group at each time point). (**E**) RT-qPCR was used to detect the changes of RSV expression in tracheal tissue of RSV infected mice ($n \ge 4$ mice in each group at each time point). *The degree of significance, *P < 0.05, *P < 0.01, *P < 0.001.

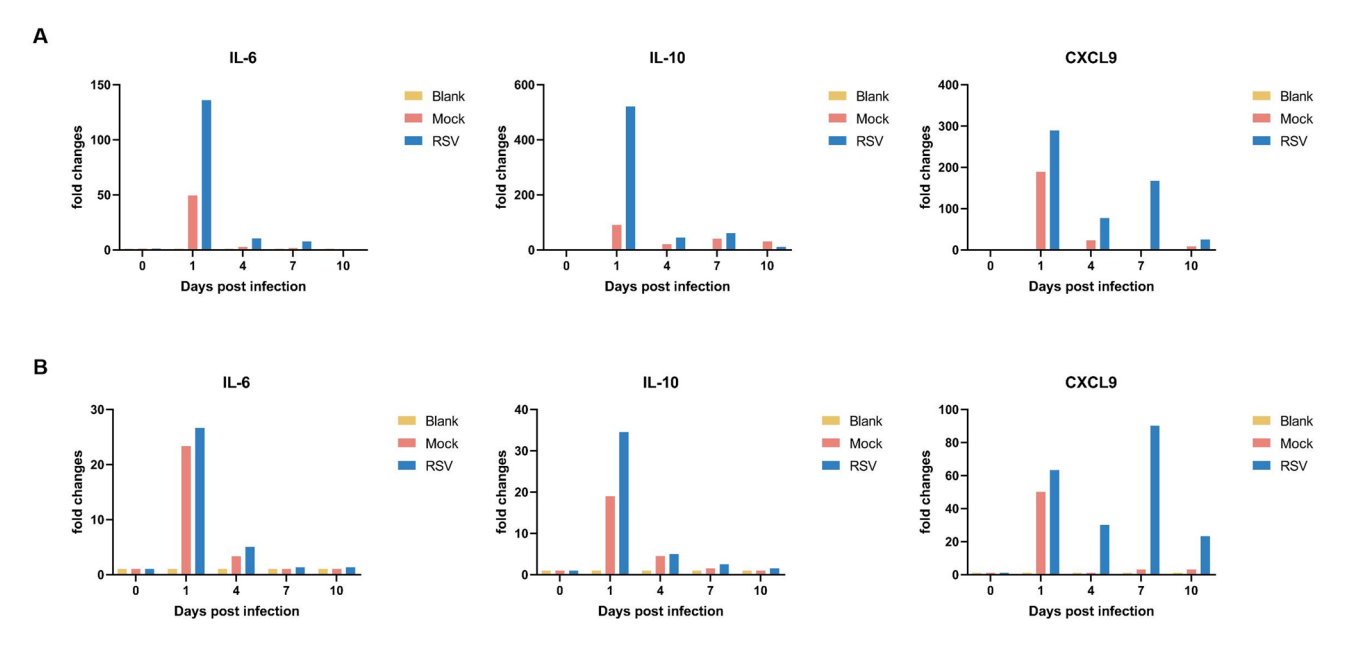


Fig. 5. RT-qPCR validation of RNA-seq data. The vertical axis represents the fold change compared to day 0, and the horizontal axis represents the time of sample collection. (A) The RNA-Seq data. (B) RT-qPCR data.

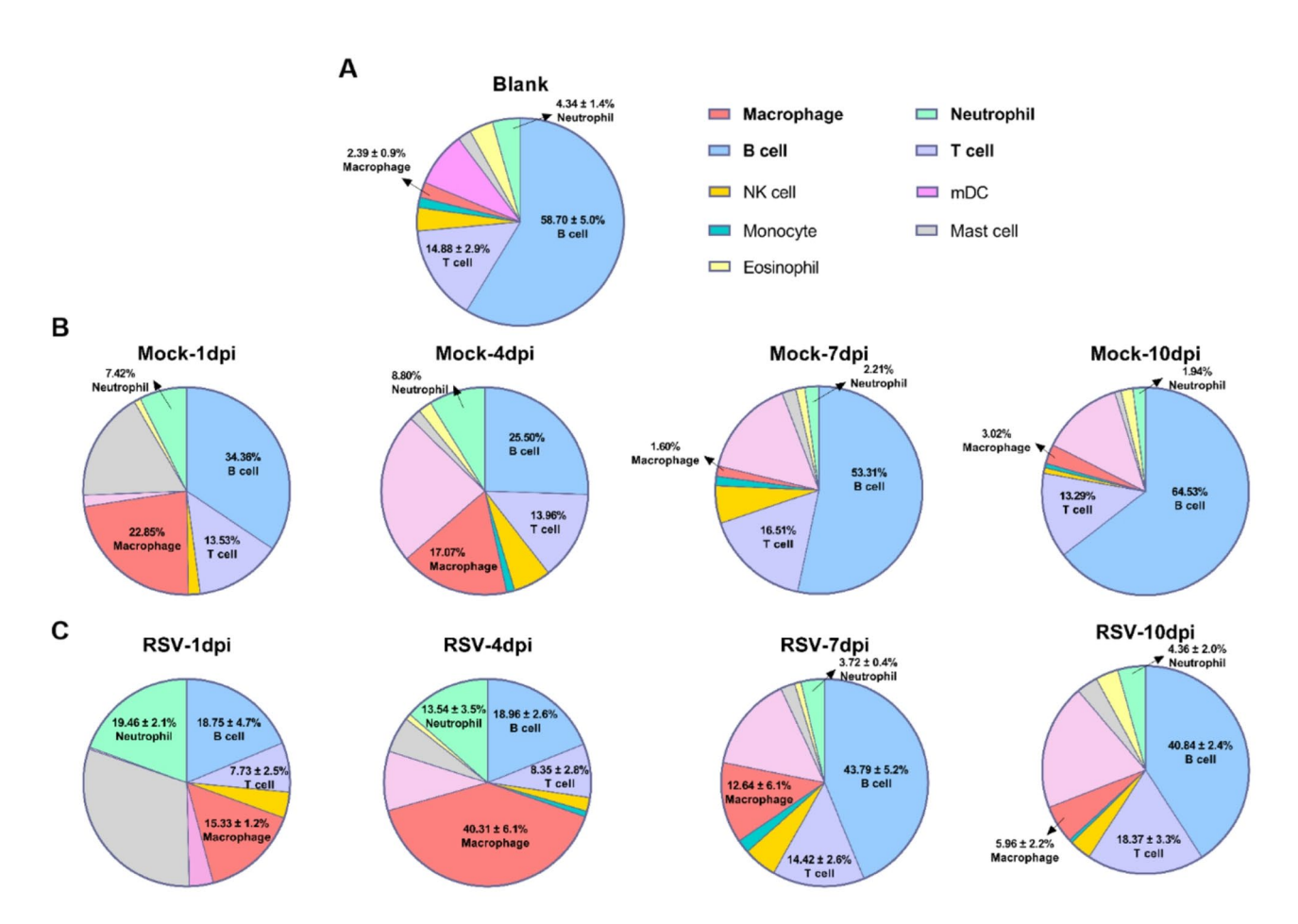


Fig. 6. Pie chart demonstrating the proportion of infiltrating immune cells. CIBERSORT was used to estimate the proportions of immune cells based on the RNA-seq gene expression profiles. The data are presented as mean \pm standard deviation (SD). (**A**) Analysis of blank group. (**B**) Analysis of mock group. (**C**) Analysis of RSV infection group.

exhibit noticeable limitations such as minimal clinical symptoms and pathology, as well as low susceptibility to the virus^{5,7}. Seemingly minor methodological differences have been demonstrated to profoundly affect the outcomes of animal studies, rendering the selection of appropriate methods critically important. In this study, we introduced the ITS infection method into mice model and compared it with the predominant INO method; interestingly, ITS resulted in more efficient viral replication and more severe pathological changes than INO. The observed significant differences in results might influence the choice of infection methods in future RSV animal experiments and ITS proves to be a suitable modeling method.

In the present study, we established and validated murine models of RSV infection using both INO and ITS methods. Comparison of data between the two modeling methods revealed that mice in the ITS method exhibited approximately twice the weight loss and significantly higher levels of viral RNA expression in lung, turbinate bone, and tracheal tissue, along with more severe H&E staining in lung tissues compared to the INO method. Thus, we concluded that ITS infection of RSV leads to more efficient virus replication and more intense pathological responses in mice. This phenomenon may be explained by the potential entry of viral inoculum into the oral cavity during INO administration, followed by expulsion through coughing reflexes, or partial ingestion into gastric tissues. In contrast, ensuring complete occlusion of the mouse's nose during ITS enables the virus solution to reach the lung tissue almost directly. In addition, the ITS approach, mimicking natural human cough action, allows the virus to quickly fill the lungs, potentially contributing to more efficient viral replication and stronger pathologic responses as well. Children, being more prone to coughing compared to adults, are more susceptible to RSV infection via coughing, potentially explaining their higher susceptibility and more severe symptoms. Therefore, ITS has also emerged as a potentially superior modeling method for simulating RSV infection in children.

In this experiment, all mice received the same batch of virus solution with identical dosage. Additionally, all animals came from the same source, were of similar age, and were housed under identical environment conditions. Therefore, except for the differences in the modeling method, other experimental conditions were sufficiently uniform to ensure a valid comparison between the two infection methods. The limitations of this study lie in focusing only on pathological changes in three respiratory tissues: lung, turbinate bone, and tracheal tissues. Studies have shown that RSV infection can affect other organs such as the spleen and

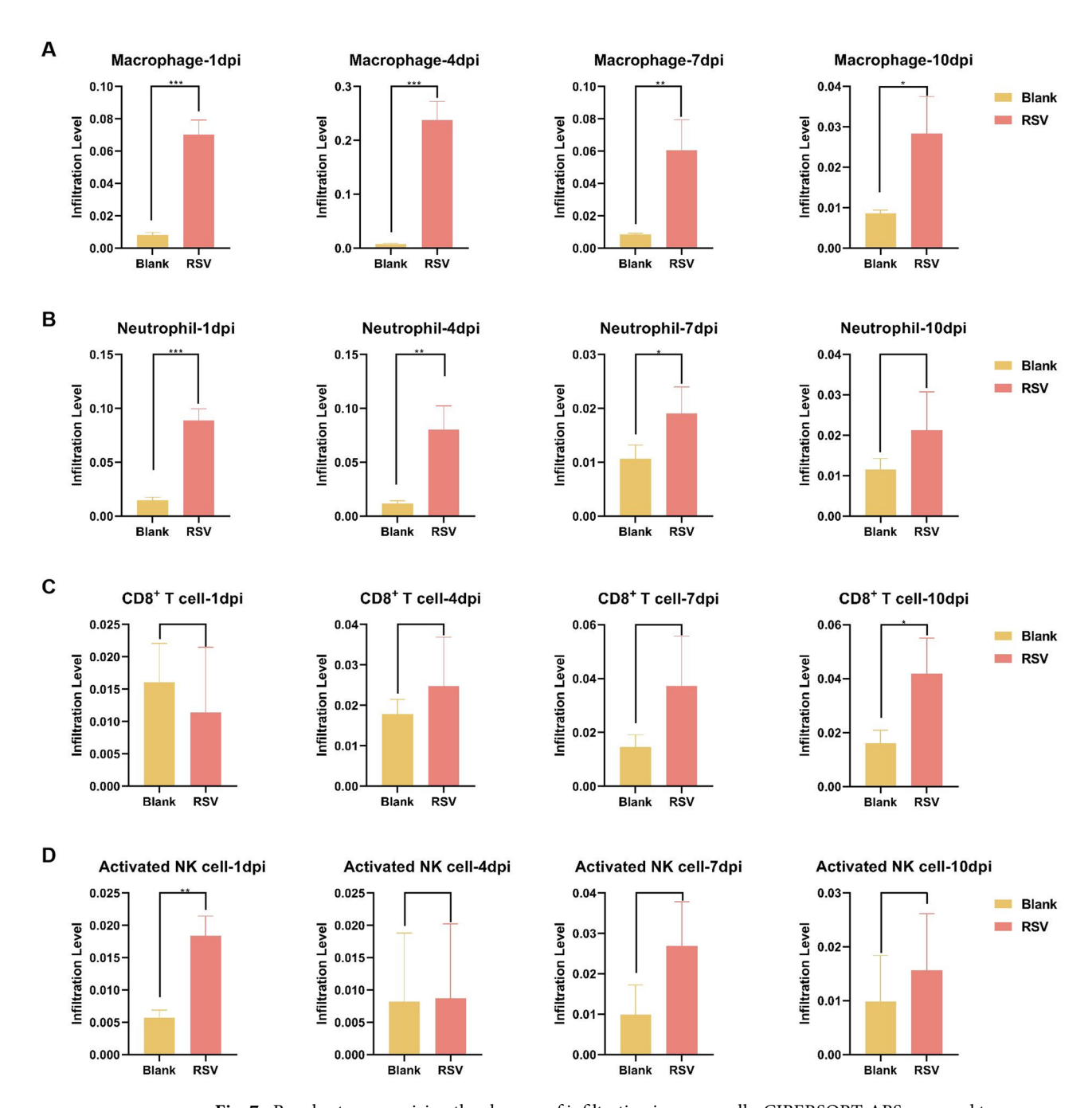


Fig. 7. Bar chart summarizing the changes of infiltrating immune cells. CIBERSORT-ABS was used to estimate the infiltration level of immune cells based on the RNA-seq gene expression profiles. (**A**) Analysis of macrophages. (**B**) Analysis of neutrophils. (**C**) Analysis of activated NK cells. (**D**) Analysis of CD8⁺ T cells. $^*P < 0.05$, $^**P < 0.01$, $^{***P} < 0.001$.

brain^{27–29}, highlighting the importance of future research on the impact of RSV via ITS method on these organs. Nonetheless, for studying the pathological changes in the mouse respiratory system post-RSV infection, the structural damage to respiratory tissues, and the pathological mechanisms in lung tissue post-infection, ITS proves to be a suitable modeling method.

Additionally, in this study, we utilized RNA-seq technology to explore transcriptional changes within the ITS modeling method and further to acquire comprehensive assessment of immune infiltration based on the extensive transcriptomic data. In this study, RT-qPCR technology was used to detect the relative expression levels of IL-6, IL-10, and CXCL9 in lung tissue RNA, and these levels were compared with the gene expression levels of IL-6, IL-10, and CXCL9 from RNA-seq data. The consistent results confirmed the accuracy of the RNA-seq data.

Subsequently, we utilized CIBERSORT and CIBERSORT-ABS algorithms to analyze immune cell infiltration in lung tissues at multiple time points. Efficient elimination of viruses requires the cooperative interaction

between innate and adaptive immunity, the two arms of the mammalian immune system. As the first line of defense, innate immunity is broadly effective, being initiated during the first few minutes of virus invasion and persisting for 3 to 4 days⁶. When the innate immunity fails to completely eliminate viruses, the adaptive immune response is usually activated 4-7 days post infection⁶. In the context of RSV, studies³⁰ have revealed that the aggregation of macrophages, neutrophils, and NK cells primarily triggers the innate immune response of the body; the aggregation of T cells and B cells constitutes the core of the adaptive immune response, as they function by recognizing specific antigens and generating immune memory. This study covered a 10-day span of RSV infection, allowing examination of both innate and adaptive immunity. Proportion analysis of infiltrating immune cells via pie charts revealed significant increase in macrophages and neutrophils at 1 and 4 days post-RSV infection and notable recovery of B cells and T cells at 7 dpi to 10 dpi. Thus, in our study, innate immune response in mouse lung tissue occurred between 1 and 4 days post-viral infection, with adaptive immune response becoming prominent from day 7 onwards. Furthermore, statistical analysis of immune cell infiltration across various types revealed significant differences in infiltration among four immune cell types. Specifically, macrophages, neutrophils and NK cells exhibited statistical differences primarily in the early infection stage, and this stage was accompanied by strong viral replication and lung immunopathological damage; CD8+ T cells demonstrated statistical differences in the late infection stage (10 dpi), when was accompanied by low viral replication and repair of lung damage. In humans, there are initial strong neutrophil responses to RSV infection which is positively correlated with disease severity, and an initial systemic T-cell lymphopenia is followed by a pulmonary CD8+ T-cell response, mediating viral clearance³¹. Therefore, major immune responses observed in humans can be modeled and replicated by the ITS approach in mice. The critical immune cell infiltration observed with ITS may be attributed to several factors. First, the direct delivery of the virus into the lungs via ITS may result in deeper viral penetration of lung tissue as you mentioned above. Second, our data showed that ITS method resulted in more efficient viral replication and more severe pathological changes than INO method, which could trigger more tissue damage and robust inflammatory response; this initial inflammatory response may recruit more immune cells, leading to the observed increase in immune cell infiltration.

In summary, RSV infection by ITS method in mice can establish effective viral infection and replication (including lung virus production and viral RNA replication in lung, turbinate bone and tracheal tissue) and cause corresponding pathological damage; the viral RNA replication and pathological change is more efficient and severe than the conventional INO method. Additionally, immunoinfiltration analysis based on transcriptomic profile demonstrated that the ITS approach can replicate major immune infiltration observed in humans, including substantial infiltration of macrophages, neutrophils, and NK cells during the early stage of RSV infection and significant infiltration of CD8⁺ T cells during later stage of RSV infection. In conclusion, intratracheal instillation of RSV is superior to intranasal inoculation as a model method in mice and can induce infiltration of important immune cells. Novel insights into the rational design of future infection methods and in vivo experiments with RSV are offered by our study, and a foundation for the investigation of the pathogenesis and immune mechanism of RSV is provided.

Data availability

The datasets generated and/or analysed during the current study are available in the Genome Sequence Archive repository in BIG Data Center (https://bigd.big.ac.cn/), under the accession number: PRJCA031383.

Received: 29 September 2024; Accepted: 20 May 2025

Published online: 04 June 2025

References

- Ca, R. Respiratory Syncytial Virus: Spectrum of Clinical Manifestations and Complications in Children. Pediatric annals, 48. (2019).
- 2. Li, Y. et al. R. investigators. Global, regional, and national disease burden estimates of acute lower respiratory infections due to respiratory syncytial virus in children younger than 5 years in 2019: a systematic analysis. *Lancet (London, England)*, 399, 2047–2064. (2022).
- 3. Ceneviva, Z. J., Norlander, A. E. & Stokes Peebles, R. Jr. Mouse models of respiratory syncytial virus infection. *Methods Mol. Biol.* **2506**, 19–41 (2022).
- 4. Bonneux, B. et al. Direct-acting antivirals for RSV treatment, a review. Antiviral Res. 229, 105948 (2024).
- De Meyer, A. & Meuleman, P. Preclinical animal models to evaluate therapeutic antiviral antibodies. Antiviral Res. 225, 105843 (2024).
- Ma, H. M. B. & Da, J. Impact of respiratory syncytial virus infection on host functions: implications for antiviral strategies. *Physiological Reviews*, 100. (2020).
- Zhang, G., Zhao, B. & Liu, J. The development of animal models for respiratory syncytial virus (RSV) infection and enhanced RSV disease. Viruses 16 (11), 1701 (2024).
- Shilovskiy, I. P., Yumashev, K. V., Nikolsky, A. A. & Vishnyakova, L. I. Khaitov. Molecular and cellular mechanisms of respiratory syncytial viral infection: using murine models to understand human pathology. Biochem. (Mosc). 86, 290–306 (2021).
- 9. Bergeron, H. C. & Tripp, R. A. RSV replication, transmission, and disease are influenced by the RSV G protein. Viruses 14 (11), 2396 (2022).
- 10. Meister, T. L. et al. Virucidal activity of oral, hand, and surface disinfectants against respiratory syncytial virus. *J. Hosp. Infect.* **141**, 25–32 (2023).
- Morales-Nebreda, L. et al. Radigan. Intratracheal administration of influenza virus is superior to intranasal administration as a model of acute lung injury. *J. Virol. Methods.* 209, 116–120 (2014).
 Capraro, G. A., Johnson, J. B., Kock, N. D. & Parks, G. D. Virus growth and antibody responses following respiratory tract infection
- of ferrets and mice with WT and P/V mutants of the paramyxovirus Simian virus 5. Virology 376, 416–428 (2008).

 13. van Erp, E. A. et al. Pathogenesis of respiratory syncytial virus infection in BALB/c mice differs between intratracheal and
- 13. van Erp, E. A. et al. Pathogenesis of respiratory syncytial virus infection in BALB/c mice differs between intratracheal and intranasal inoculation. Viruses 11, 508 (2019).
- Li, J. et al. Yi. Tangeretin attenuates bleomycin-induced pulmonary fibrosis by inhibiting epithelial-mesenchymal transition via the PI3K/Akt pathway. Front. Pharmacol. 14, 1247800 (2023).

- 15. Zhou, Q. et al. Intratracheal instillation of high dose adenoviral vectors is sufficient to induce lung injury and fibrosis in mice. *PLoS One*, **9**, e116142. (2014).
- Westermann, A. J. & Vogel, J. Cross-species RNA-seq for Deciphering host-microbe interactions. Nat. Rev. Genet. 22, 361–378 (2021).
- 17. Li, T. et al. TIMER2.0 for analysis of tumor-infiltrating immune cells. Nucleic Acids Res. 48 (W1), W509-W514 (2020).
- 18. He, Y. et al. Exploring key genes and mechanisms in respiratory syncytial Virus-Infected BALB/c mice via Multi-Organ expression profiles. Front. Cell. Infect. Microbiol. 12, 858305 (2022).
- 19. Yao, W. et al. Cai. The cellular and viral circrnaome induced by respiratory syncytial virus infection. mBio 12, e0307521 (2021).
- 20. Newman, A. M. et al. Alizadeh. Robust enumeration of cell subsets from tissue expression profiles. *Nat. Methods.* **12**, 453–457 (2015).
- 21. Meng, X. Y. et al. Fan. A novel animal model of primary blast lung injury and its pathological changes in mice. *J. Trauma. Acute Care Surg.* **93**, 530–537 (2022).
- Salimi, V. et al. Evaluation of the expression level of 12/15 Lipoxygenase and the related inflammatory factors (CCL5, CCL3) in respiratory syncytial virus infection in mice model. Microb. Pathog. 109, 209–213 (2017).
- Nuriev, R. & Johansson, C. Chemokine regulation of inflammation during respiratory syncytial virus infection. F1000Res 8, F1000FacultyRev-1837 (2019).
- 24. Qi, F. et al. Liu. Respiratory macrophages and dendritic cells mediate respiratory syncytial virus-induced IL-33 production in TLR3- or TLR7-dependent manner. *Int. Immunopharmacol.* 29, 408–415 (2015).
- 25. [25]Langedijk, A. Ĉ. & Bont, L. J. Respiratory syncytial virus infection and novel interventions. Nat Rev Microbiol. ;21(11):734–749. (2023). https://doi.org/10.1038/s41579-023-00919-w. Epub 2023 Jul 12. Erratum in: Nat Rev Microbiol. 2024 Sep.
- Mazur, N. I. et al. Zambon, L. Bont. Respiratory syncytial virus prevention within reach: the vaccine and monoclonal antibody landscape. Lancet Infect. Dis. 23, e2–e21 (2023).
- 27. He, Y. et al. Exploring Key Genes and Mechanisms in Respiratory Syncytial Virus-Infected BALB/c Mice via Multi-Organ Expression Profiles. Front Cell Infect Microbiol. May 2. (2022).
- 28. Chiriboga-Salazar, N. R. & Hong, S. J. Respiratory syncytial virus and influenza infections: the brain is also susceptible. *J. Pediatr.* (2021) Dec.
- Liu, W. et al. Epidemiology and clinical presentations of respiratory syncytial virus subgroups A and B detected with multiplex Real-Time PCR. PLoS One Oct 20. (2016).
- 30. Bergeron, H. C. & Tripp, R. A. Immunopathology of RSV: an updated review. Viruses Dec 10. (2021).
- 31. Russell, C. D., Unger, S. A., Walton, M. & Schwarze, J. The human immune response to respiratory syncytial virus infection. *Clin Microbiol. Rev* (2017) Apr.

Author contributions

W.X., Z.L., Y.X. and Y.L. contributed to conception and design of the study; B.P., M.X., Y.X. and Y.L. conducted the experiment.; Z.M. and M.L. collected the data; B.P., M.X., Y.X. and Y.L. organized the data; S.M., X.Y. and W.L. organized the figure; Y.W., W.Y. and Z.L. performed the ststistical analysis; Y.L. and Y.X. wrote the main manuscript text. All authors contributed to manuscript revision, read and approved the submitted version.

Funding

This work was supported by grants from the National Natural Science Foundation of China (32270153), Key Laboratory of Guangdong Higher Education Institutes (2021KSYS009), the Science and Technology Program of Guangzhou (202102010128, 2024A04J8217 and 2024A03J0077), Guangzhou Key Laboratory of Biological Targeting Diagnosis and Therapy (202201020379), and Open Project of State Key Laboratory of Respiratory Disease (SKLRD-OP-202323).

Declarations

Competing interests

The authors declare no competing interests.

Ethical statement

All animal studies were conducted according to ethical standards and approved by the relevant national authorities.

Additional information

Supplementary Information The online version contains supplementary material available at https://doi.org/1 0.1038/s41598-025-03521-7.

Correspondence and requests for materials should be addressed to Z.L. or W.Y.

Reprints and permissions information is available at www.nature.com/reprints.

Publisher's note Springer Nature remains neutral with regard to jurisdictional claims in published maps and institutional affiliations.

Open Access This article is licensed under a Creative Commons Attribution-NonCommercial-NoDerivatives 4.0 International License, which permits any non-commercial use, sharing, distribution and reproduction in any medium or format, as long as you give appropriate credit to the original author(s) and the source, provide a link to the Creative Commons licence, and indicate if you modified the licensed material. You do not have permission under this licence to share adapted material derived from this article or parts of it. The images or other third party material in this article are included in the article's Creative Commons licence, unless indicated otherwise in a credit line to the material. If material is not included in the article's Creative Commons licence and your intended use is not permitted by statutory regulation or exceeds the permitted use, you will need to obtain permission directly from the copyright holder. To view a copy of this licence, visit https://creativecommons.org/licenses/by-nc-nd/4.0/.

© The Author(s) 2025